frontiers in Chemistry

ORIGINAL RESEARCH
published: 02 March 2021
doi: 10.3389/fchem.2021.574722

Thermodynamics and Kinetics of Sulfuric Acid Leaching Transformation of Rare Earth Fluoride Molten Salt Electrolysis Slag

Lijie Chen, Jiacong Xu, Xiaoqiang Yu, Lei Tian, Ruixiang Wang* and Zhifeng Xu**

Institute of Green Metallurgy and Process Intensification, Jiangxi University of Science and Technology, Ganzhou, China

OPEN ACCESS

Edited by:
Doo Soo Chung,
Seoul National University, South Korea

Reviewed by:
Shili Zheng,
Institute of Process Engineering (CAS), China
Yi Zhang,
Nanjing Tech University, China

****Correspondence:***
Lei Tian
tianleijx@163.com
Ruixiang Wang
wrx9022@163.com
Zhifeng Xu
xu.zf@jxust.edu.cn

Specialty section:
This article was submitted to Physical Chemistry and Chemical Physics, a section of the journal Frontiers in Chemistry

Received: *23 June 2020*
Accepted: *04 January 2021*
Published: *02 March 2021*

Citation:
Chen L, Xu J, Yu X, Tian L, Wang R and Xu Z (2021) Thermodynamics and Kinetics of Sulfuric Acid Leaching Transformation of Rare Earth Fluoride Molten Salt Electrolysis Slag. Front. Chem. 9:574722. doi: 10.3389/fchem.2021.574722

Rare earth element recovery in molten salt electrolysis is approximately between 91 and 93%, whereof 8% is lost in waste molten salt slag. Presently, minimal research has been conducted on the technology for recycling waste rare earth molten salt slag, which is either discarded as industrial garbage or mixed with waste slag into qualified molten salt. The development of a new approach toward the effective treatment of rare earth fluoride molten salt electrolytic slag, which can recycle the remaining rare earth and improve the utilization rate, is essential. Herein, weak magnetic iron separation, sulfuric acid leaching transformation, water leaching, hydrogen fluoride water absorption, and cycle precipitation of rare earth are used to recover rare earth from their fluoride molten salt electrolytic slag, wherein the thermodynamic and kinetic processes of sulfuric acid leaching transformation are emphatically studied. Thermodynamic results show that temperature has a great influence on sulfuric acid leaching. With rising temperature, the equilibrium constant of the reaction gradually increases, and the stable interval of NdF_3 decreases, while that of Nd^{3+} increases, indicating that high temperature is conducive to the sulfuric acid leaching process, whereof the kinetic results reveal that the activation energy E of Nd transformation is 41.57 kJ/mol, which indicates that the sulfuric acid leaching process is controlled by interfacial chemical reaction. According to the Nd transformation rate equation in the sulfuric acid leaching process of rare earth fluoride molten salt electrolytic slag under different particle size conditions, it is determinable that with the decrease of particle size, the reaction rate increases accordingly, while strengthening the leaching kinetic process. According to the equation of Nd transformation rate in the sulfuric acid leaching process under different sulfuric acid concentration conditions, the reaction series of sulfuric acid concentration $K = 6.4$, which is greater than 1, indicating that increasing sulfuric acid concentration can change the kinetic-control region and strengthen the kinetic process.

Keywords: rare earth, sulfuric acid leaching transformation, thermodynamics, kinetics, interfacial chemical reaction

INTRODUCTION

The focus of world research gradually tends to functional materials (Gao et al., 2020; Kong et al., 2020; Zhang et al., 2020; Zhang et al., 2021), rare earth and its compounds have excellent physical and chemical properties, such as electricity, magnetism, light, and catalysis, which make them widely used in metallurgy, chemical industry, electronics, machinery, new energy, new materials, aerospace, and other fields (Huang et al., 2007; Biedermann, 2014; Shen et al., 2017). The utilization rate of rare earth resources in the world is only approximately 10%, which is evidently not directly proportional to the value of rare earth. For these kinds of nonrenewable, scarce, and strategic resources, it is of great significance to recycle and reuse the rare earth in them (Chen, 2011; Huang et al., 2015; Ferron and Henry, 2016)[8–10].

Rare earth elements are very active, making their extraction from waste compounds via common methods difficult. In industrial production, rare earth chlorides, oxides, and fluorides are the main materials for preparing rare earth metals. The main methods used are metal thermal reduction and molten salt electrolysis. Presently, lanthanum, praseodymium, neodymium, dysprosium, and other single rare earth metals, as well as Pr-Nd, Nd-Fe, Dy-Fe, and other alloys are all produced by the molten salt electrolysis process of the fluoride system (Li, 1990). In the actual production process, many non-rare earth impurities accumulate in the rare earth molten salt. During rare earth metal discharging and anode changing, the rare earth molten salt can be easily released, thereby causing pollution. Some polluted rare earth molten salts will also be produced during the process of regular furnace cleaning and dismantling. Currently, an increasing number of experts and scholars, locally and globally, are studying the recovery and utilization technology of rare earth molten salt electrolytic slag because of its high rare earth content and great reuse value (Chen et al., 2005; Xiao et al., 2015; Federica et al., 2019; Onal and Binnemans, 2019; Yurramendi et al., 2019).

At present, the most commonly used approach toward rare earth molten salt electrolytic slag is to add flux (SiO_2, $Na_2B_4O_7$, and $Ca(OH)_2$) and mix with rare earth molten salt electrolytic slag for roasting, after which dilute acid or water is used to leach the soluble rare earth in the roasting slag, and finally separating and enriching the rare earth via extraction or selective precipitation. He, 2016 employed the mixed roasting of H_2SO_4 and SiO_2, sulfuric acid leaching, hydrolysis, as well as the removal of rare earth impurities, ammonium bicarbonate, and precipitation to treat the electrolytic slag of rare earth fluoride molten salt, and finally obtained a neodymium carbonate product. The results showed that in the process of roasting and leaching, the electrolytic residue (g): H_2SO_4 (ML) was 1: 1.6, the electrolytic residue (g): SiO_2 (g) was 1:0.15, the roasting temperature was 973 K, the roasting time was 1.5 h, and the leaching rate reached 90.36%. During precipitation, the pH value is 6–6.5, the time is 50 min, the precipitation is complete at 318 K, and the total rare earth recovery is 88%. Yang et al. (2020) proposed a new method of borax roasting followed by hydrochloric acid leaching to extract rare earth from rare earth molten salt electrolytic slag. The results show roasting the slag at 973 K for 60 min with a borax mass dosage of 38 wt.% and subsequently leaching the resulting rare earth-containing residues in 4 mol L^{-1} HCl at 60°C at a liquid/solid ratio of 5:1 for 40 min. These conditions gave a rare earth recovery exceeding 97%. Lin et al., 2012 initially smashed rare earth metal molten salt electrolytic waste, then added calcium hydroxide for batching, put it into a muffle furnace for sintering, remove the sintering slag and dissolve it with hydrochloric acid, extract and separate the obtained lixivium with P507, perform carbonate precipitation for the lixivium after stripping, and burned the precipitate to obtain rare earth oxide products; this process can produce a single rare earth oxide, among which the fluorine content of the raw materials is replaced to form calcium fluoride. The recovery rate of rare earth oxide is 94.44% when the weight ratio of rare earth metal molten salt electrolysis waste to calcium hydroxide is 1:0.5, the reaction temperature is 950°C, and the reaction time is 3.5 h. Liang et al., 2018 invented a new method to extract rare earth from the molten salt electrolytic slag of rare earth in a fluoride salt system. This method entailed the mixing of sodium silicate and rare earth molten salt electrolytic slag, and the rare earth material solution is obtained through high temperature roasting, water immersion, filtration, and reaction with hydrochloric acid. The experimental results show that the mass ratio of molten salt electrolytic slag and silicate in the fluoride system is 1:1.2, the roasting time is 1.5 h, the roasting temperature is 1173 K, the hydrochloric acid concentration is 1.5 mol/L, the reaction temperature between the roasting product and hydrochloric acid is 323 K, the reaction time is 1.0 h, and the rare earth leaching rate exceeds 99%. Some experts also use the high stability of rare earth fluoride to remove the impurities in the molten salt electrolytic slag by dilute acid leaching. The leaching slag can be directly returned to the molten salt electrolytic cell for the preparation of rare earth metals. Xiao et al., 2015 utilized the non-reactive rare earth fluoride characteristic with hydrochloric

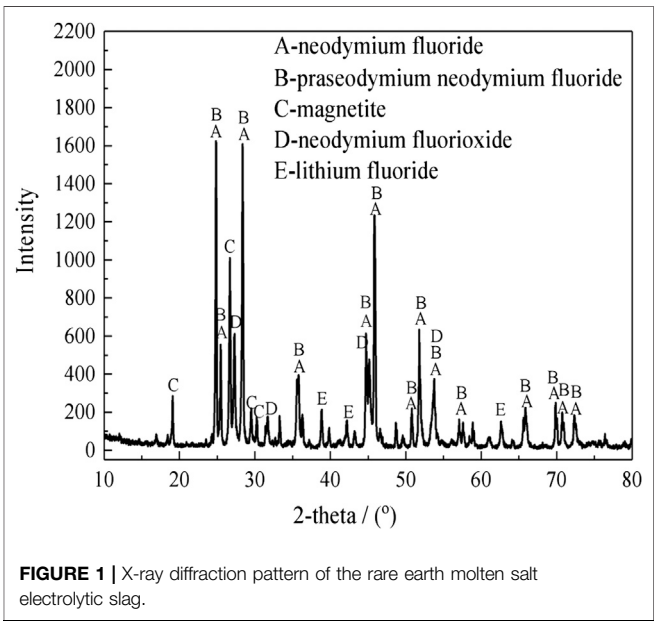

FIGURE 1 | X-ray diffraction pattern of the rare earth molten salt electrolytic slag.

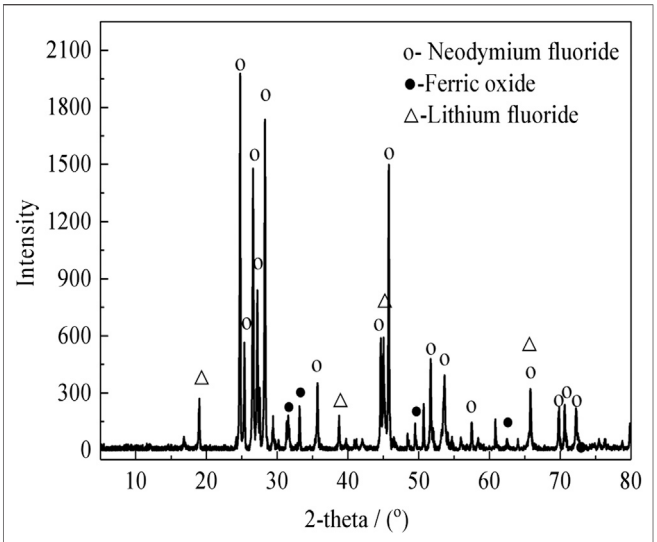

FIGURE 2 | XRD analysis of non-magnetic fraction.

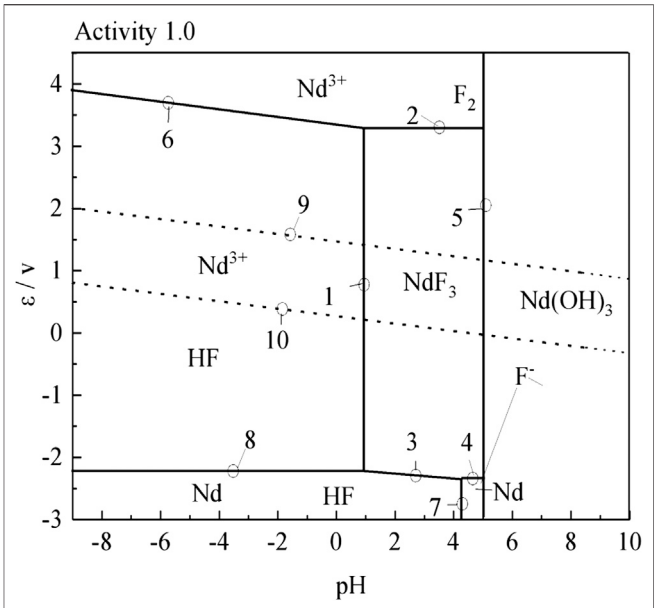

FIGURE 4 | ε-pH diagram of the Nd-F-H_2O system with different activities at 573 K.

acid, used hydrochloric acid leaching to dissolve and leach the soluble non-rare earth impurities and soluble rare earth compounds in the electrolytic waste of rare earth praseodymium neodymium molten salt, and recovered them to obtain rare earth fluoride and rare earth oxide. The results show that when the abrasive particle size is −200 meshes, the temperature is 50°C, hydrochloric acid is added to the final system to keep the pH value at 0.5, and the reaction time is 4 h, the removal rate of main non-rare earth metal impurities in the waste slag is over 94%, and the total recovery rate of rare earth is 97.56%.

It is evident from the above-mentioned literature that regardless of flux addition to calcine or using dilute acid to remove impurities in slag, good rare earth utilization rates are achievable, but the waste slag and waste water generated by these methods need to be treated, and the fluorine ions in them remain unused, which is capable of causing environmental degradation. Therefore, the methods of weak magnetic separation, sulfuric acid ripening transformation, water immersion, HF water absorption, and rare earth circulation settling are used to recover rare earth in the molten salt electrolytic slag of rare earth fluoride. This paper focuses on the thermodynamics and dynamic process of sulfuric acid ripening transformation of the slag of molten salt electrolysis of rare earth fluoride, solves the problem of separating rare earth from fluorine in the molten salt electrolytic slag of rare earth, and realizes the green recovery of rare earth from the slag of molten salt electrolysis of rare earth production and efficient recovery provide a technical basis for the recovery and utilization of rare earth molten salt electrolytic slag.

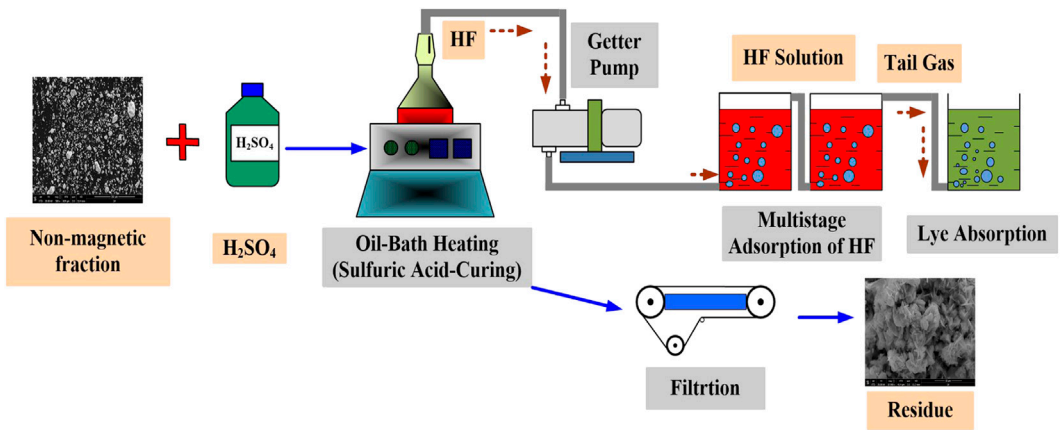

FIGURE 3 | Process of fluoride sulfate conversion.

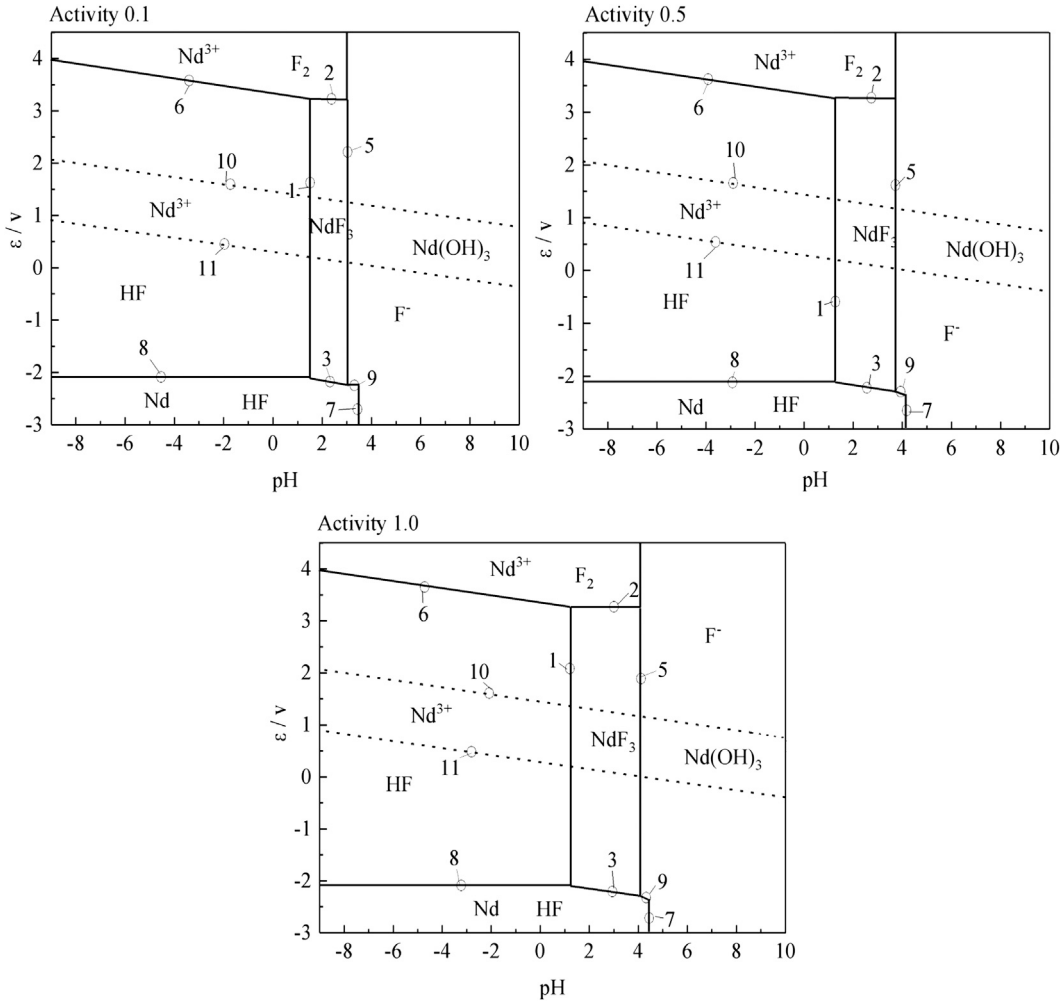

FIGURE 5 | ε-pH diagram of the Nd-F-H_2O system with different activities at 603 K

MATERIALS AND METHODS

Materials

The rare earth molten salt electrolytic slag was obtained from Ganzhou, Jiangxi, China. The non-magnetic fraction of the rare earth molten salt electrolytic slag after magnetic separation is used as the experimental material. The bulk chemical composition was measured. The results show that the samples contain 52.8 wt% Nd, 32.3 wt% F, 7.1 wt% Li, 0.6 wt% Si, 4.2 wt% O, 2.9 wt% Fe, and other elements. The X-ray diffraction (XRD) pattern analysis of the rare earth molten salt electrolytic slag and the non-magnetic fraction are shown in **Figure 1** and **Figure 2**, respectively.

As shown in **Figure 1**, the XRD analysis shows that the main mineralogical phase in the rare earth molten salt electrolytic slag are NdF_3, $(Nd,Pr)F_3$, NdOF, LiF and Fe_3O_4. As shown in **Figure 2**, The rare earth phase in non-magnetic fraction exists in the form of rare earth fluoride, and there are also small amounts of hematite, limonite, olivine, and occasionally magnetite.

Experimental Procedure

The sample (non-magnetic fraction) and sulfuric acid of different concentrations were mixed at a certain ratio, and then placed in a thermostatic oil bath; The effects of temperature, liquid–solid ratio, aging time, and sulfuric acid concentration on aging effects were investigated by controlling the conditions. The generated hydrogen fluoride gas was recycled by multistage adsorption and dissolved in water. After the aging reaction was completed, the filtrate and filter residue were collected and analyzed. The fluoride sulfate conversion process is shown in **Figure 3**.

RESULTS AND DISCUSSION

Drawing of Potential pH Diagram of Nd-F-H_2O System

Drawing of ε-pH Diagram of Nd-F-H_2O System at Different Temperatures and Activities

According to the results of the reaction formula in **Table 1**, the ε-pH diagram of the Nd-F-H_2O system at a temperature of

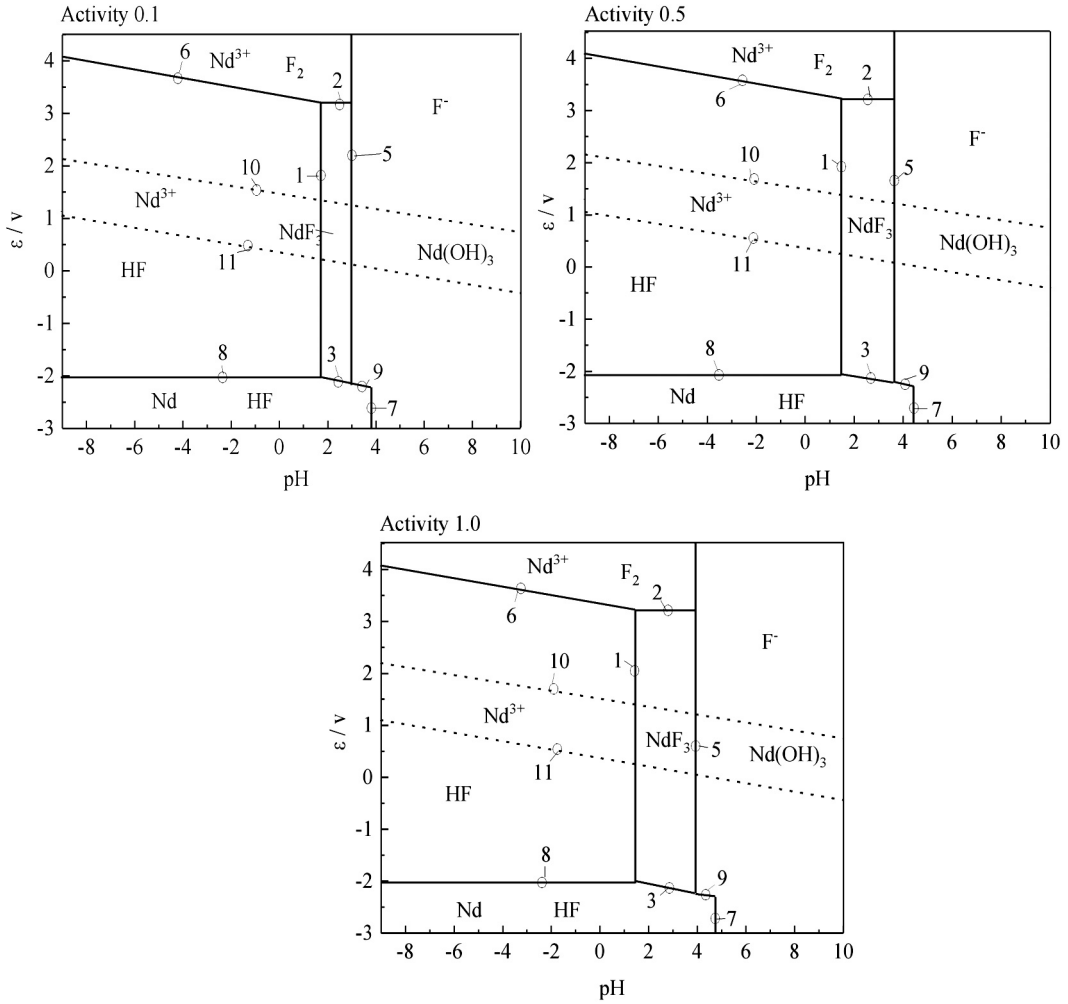

FIGURE 6 | ε-pH diagram of the Nd-F-H_2O system with different activities at 633 K.

573–663 K and activity of 0.1, 0.5, and 1.0 is drawn, as shown in **Figures 4–7**.

The stable zone of HF and Nd^{3+} was determined from the ε-pH diagram, and the reaction conditions were controlled so that NdF_3 could be converted into HF and Nd^{3+} as much as possible to ensure the smooth progress of sulfuric acid leaching reaction.It can be seen from **Figures 4–7** that with the increase of temperature and activity, the stability area of HF significantly increased. Although the stable area of Nd^{3+} also increases, the change is relatively insignificant. In summary, the improvement of temperature and activity is conducive to the enlargement of the stable area of HF and Nd^{3+} to promote the reaction.

ε-pH Diagram Guidance for Temperature Selection

To compare the stable regions of various substances in the sulfuric acid curing process at different temperatures, the ε-pH diagram of the Nd-F-H_2O system at different temperatures is listed, and the results are shown in **Figure 8**.

According to **Figure 8**, as the temperature increases, the stable range of NdF_3 becomes smaller, while that of Nd^{3+} becomes larger, and the kinetic conditions of high temperature reactions are more favorable. The equilibrium constants of the stable region for the formation of Nd^{3+} by the acid dissolution of NdF_3 are shown in **Table 2**. It can be seen that with a rise in temperature, the equilibrium constant of the reaction gradually increases. Compared with the stable region of Nd^{3+} in the potential pH diagram, high temperature has a better leaching effect.

Kinetic Experiment of Sulfuric Acid Curing

Effect of Particle Size on Transformation of Nd

Under acid concentration conditions of 98%, temperature of 633 K, liquid–solid ratio of 50:1, and a constant stirring speed of 300 r min^{-1}, the effects of the particle size on Nd transformation is observed. The results, which reveal that Nd transformation rate increases with a decrease in granularity, are shown in **Figure 9A**. Especially in the initial 5 min of ripening, the transformation effect is very obvious, but after 5 min of leaching, the growth trend apparently reduces because the active NdF and NdOF in the sample have basically reacted completely in a short time.

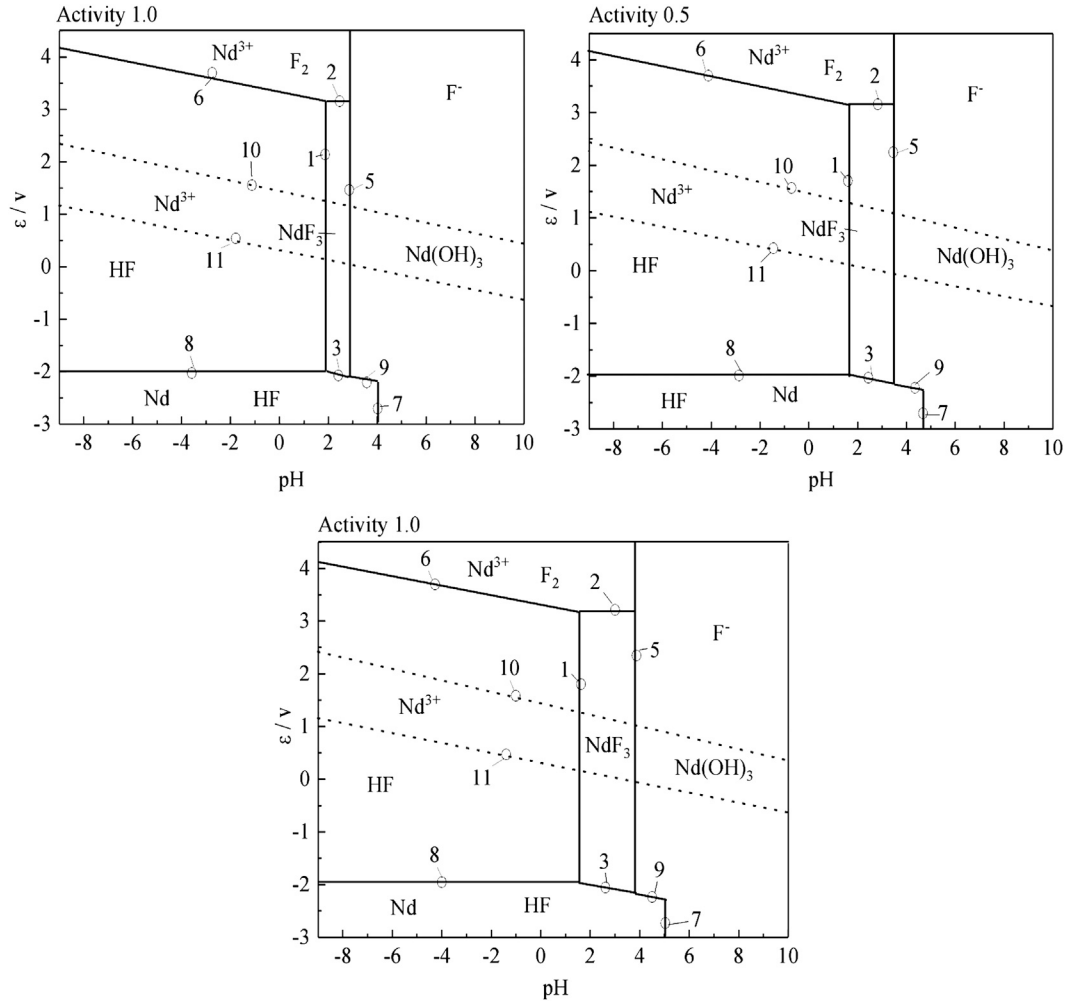

FIGURE 7 | ε-pH diagram of the Nd-F-H_2O system with different activities at 663 K.

Effect of Temperature on Transformation of Nd

Under acid concentration conditions of 98%, a particle size of 58–75 μm, a liquid–solid ratio of 50:1, and a constant stirring speed of 300 r min^{-1}, the effects of temperature on the Nd transformation is observed. The results are shown in **Figure 9B**. The results show that the Nd transition rate increases as the temperature rises. Especially, when the curing temperature exceeds 633 K, the transformation rate of the final Nd is over 95%.

Effect of H_2SO_4 Concentration on Transformation of Nd

Under temperature conditions of 633 K, a particle size of 58–75 μm, a liquid–solid ratio of 50:1, and a constant stirring speed of 300 r min^{-1}, the effects of temperature on the Nd transformation is observed. The results, which revealed that Nd transformation rate increased with the increase of sulfuric acid concentration, are shown in **Figure 9C**. When the concentration of sulfuric acid is 98%, the effect is the best, and the transformation rate of Nd reaches over 95% after 180 min of leaching.

Kinetic Modeling

Kinetic experiments were conducted according to the conditions of the sulfuric acid curing processes. In sulfuric acid curing, the sulfuric acid concentration can be considered as constant with sufficiently large liquid-to-solid ratio and stirring. **Figure 10** shows a scanning electron microscopy (SEM) micrograph of the sample and sulfuric acid transition residue.

The SEM micrographs (**Figure 10A**) of the sample show that the particle surfaces are loose and porous, and the surface is covered with fine particles. **Figure 10B** shows that the size of the sulfuric acid transition residue is consistent with the sample, but the particles are fluffier and more porous. The relevant empirical equations (Baláz, 2003; Sokic et al., 2009) were fitted (the data from **Figure 9B**. The results of their correlation coefficients show that the Erofejev–Kolmogorov kinetic equation has the best linear

TABLE 1 | Reaction in Nd-F-H_2O system at 573–663 K and calculation formula of ε and pH.

Reaction formula	Calculation formula of ε and pH			
1. $NdF_3+3H^+ = Nd^{3+}+3HF$	pH_{573} = 0.933–0.333 lga_{Nd}^{3+}	pH_{603} = 1.177–0.333 lga_{Nd}^{3+}	pH_{633} = 1.387–0.333 lga_{Nd}^{3+}	pH_{663} = 1.553–0.333 lga_{Nd}^{3+}
2. $Nd^{3+}+3F_2+6e^- = 2NdF_3$	ε_{573} = 3.317 + 0.020 lga_{Nd}^{3+}	ε_{603} = 3.283 + 0.023 lga_{Nd}^{3+}	ε_{633} = 3.246 + 0.026 lga_{Nd}^{3+}	ε_{663} = 3.208 + 0.030 lga_{Nd}^{3+}
3. $NdF_3+3H^++3e^- = Nd+3HF$	ε_{573} = −2.065–0.059 pH	ε_{603} = −1.988–0.069 pH	ε_{633} = −1.905–0.079 pH	ε_{663} = −1.817–0.089 pH
4. $NdF_3+3e^- = Nd+3F^-$	ε_{573} = −2.315–0.059 lga_{F^-}	ε_{603} = −2.295–0.069 lga_{F^-}	ε_{633} = −2.276–0.079 lga_{F^-}	ε_{663} = −2.263–0.089 lga_{F^-}
5. $Nd(OH)_3+3H^++3F^- = NdF_3+3H_2O$	pH_{573} = 5.058+lga_{F^-}	pH_{603} = 4.023+lga_{F^-}	pH_{633} = 3.900+lga_{F^-}	pH_{663} = 3.790+lga_{F^-}
6. $F_2+2H^++2e^- = 2HF$	ε_{573} = 3.372–0.059 pH	ε_{603} = 3.364–0.069 pH	ε_{633} = 3.364–0.079 pH	ε_{663} = 3.364–0.089 pH
7. $H++F^- = HF$	pH_{573} = 4.240+lga_{F^-}	pH_{603} = 4.450+lga_{F^-}	pH_{633} = 4.701+lga_{F^-}	pH_{663} = 4.994+lga_{F^-}
8. $Nd_3^++3e^- = Nd$	ε_{573} = −2.120+0.020 lga_{Nd}^{3+}	ε_{603} = −2.069 + 0.023 lga_{Nd}^{3+}	ε_{633} = -2.041 + 0.0236 lga_{Nd}^{3+}	ε_{663} = −1.995 + 0.030 lga_{Nd}^{3+}
9. $Nd(OH)_3+4H++F^-+3e$-= Nd + $HF+3H_2O$	ε_{573} = −1.998–0.059 pH	ε_{603} = −1.896–0.069 pH	ε_{633} = −1.883–0.079 pH	ε_{663} = −1.796–0.089 pH
10. $O_2+4H++4e^- = 2H_2O$	ε_{573} = 1.495–0.059 pH	ε_{603} = 1.474–0.069 pH	ε_{633} = 1.497–0.079 pH	ε_{663} = 1.480–0.089 pH
11. $2H^++2e^- = H_2$	ε_{573} = 0.266–0.059 pH	ε_{603} = 0.301–0.069 pH	ε_{633} = 0.336–0.079pH	ε_{663} = 0.373–0.089pH

correlation. This equation is therefore used to analyze the sulfuric acid curing behavior. The kinetic equation of the interface (contracting tabular) can be expressed as:

$$Kt^n = -1n(1-\alpha) \quad (1)$$

where, k is the apparent rate constant, α is the fraction of neodymium converted (percentage/100), and t is the leaching time (min).

The value of n can be calculated according to the experimental data obtained in **Figure 9**, and finally n = 0591 in the sulfuric acid curing process can be obtained.

Leaching Regular Pattern Under Different Temperatures

Figure 11A shows the plots of -ln(1-α) as a function of time at different temperatures for sulfuric acid curing.

The Arrhenius plots are shown in **Figure 11B**, indicating that the transformation ratio of Nd plots are linear, over the entire temperature range. The apparent activation energies are determined, using **Eq. (5)** (Tian et al., 2018):

$$K = A_0 \exp(-E/RT) \quad (2)$$

where, k is the apparent rate constant, A_0 is the pre-exponential factor, E is the apparent activation energy (kJ/mol), T is the reaction temperature (K), and R is the universal gas constant (8.314 J mol^{-1} K^{-1}). The activation energy of the Nd transformation ratio was determined to be 41.57 kJ/mol, which means the Nd sulfate transformation process was controlled by surface chemical reaction, and the kinetic equations about the effect of temperature on Nd transformation ratio can be obtained as **Eq. (8)** :

$$1nk = 5.74 - 5.01 \times 10^3 T^{-1} \quad (3)$$

Leaching Regular Pattern Under Different Particle Size

Figure 12A shows the plots of -ln(1-α) as a function of time at different particle sizes for sulfuric acid curing. According to the fitting results of **Figure 12A**, to plotting the apparent rate constant (k) vs. the countdown of the particle size ($1/r_0$), the results can be shown in **Figure 12B**. The kinetic equations about the effect of the particle size on Nd transformation ratio can be obtained as **Eq. (4)**:

$$k = -0.013 + 7.03 r_0^{-1} \quad (4)$$

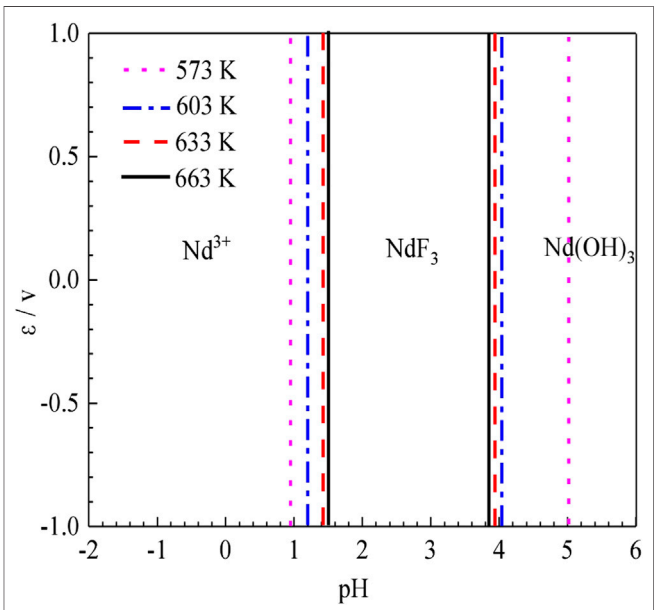

FIGURE 8 | ε-pH diagram of the Nd-F-H_2O system with activity 1 at different temperatures.

TABLE 2 | Comparison of equilibrium constants of Nd^{3+} region generated by NdF_3 at different temperatures.

temperature/K	K_1^0
573	632.105
603	3410.9
633	14,498.9
663	45,611.9

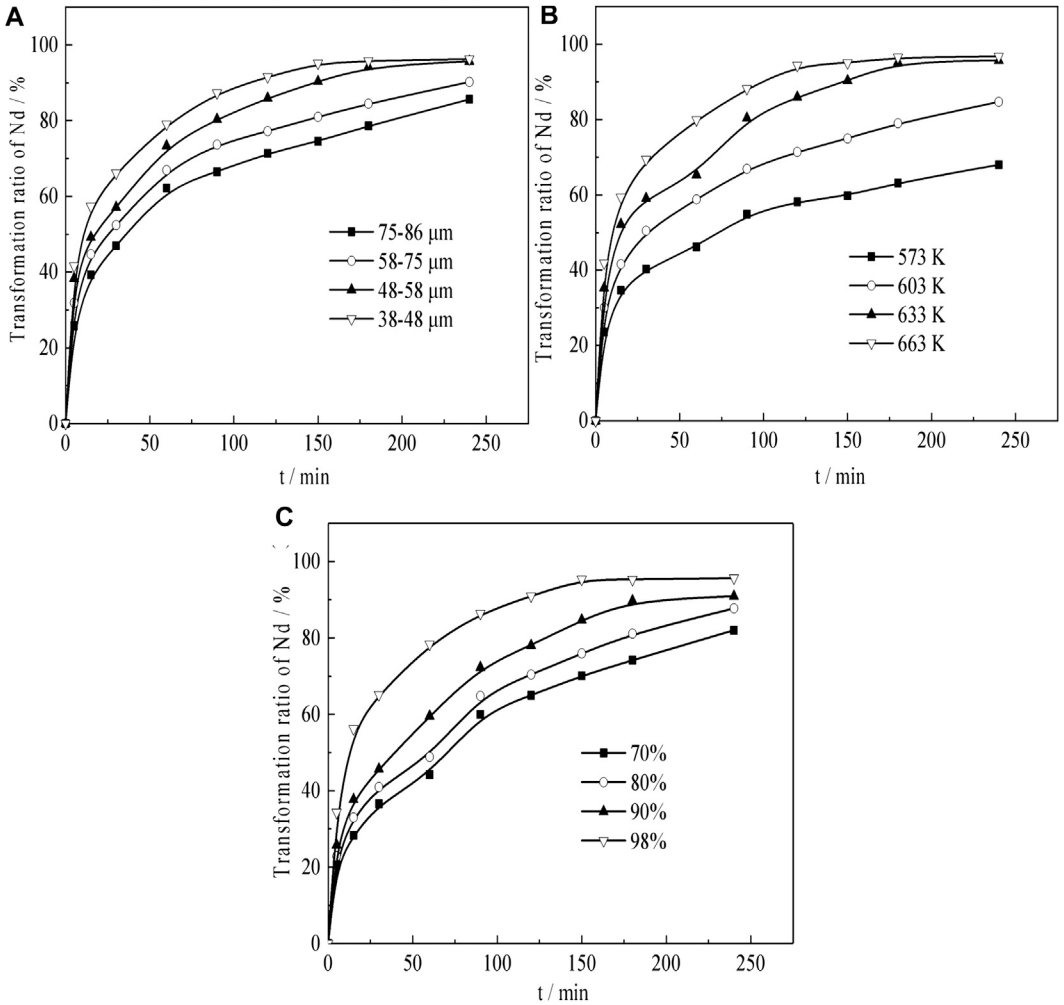

FIGURE 9 | Effect of **(A)** particle size, **(B)** temperature, and **(C)** H_2SO_4 concentration on Nd transformation.

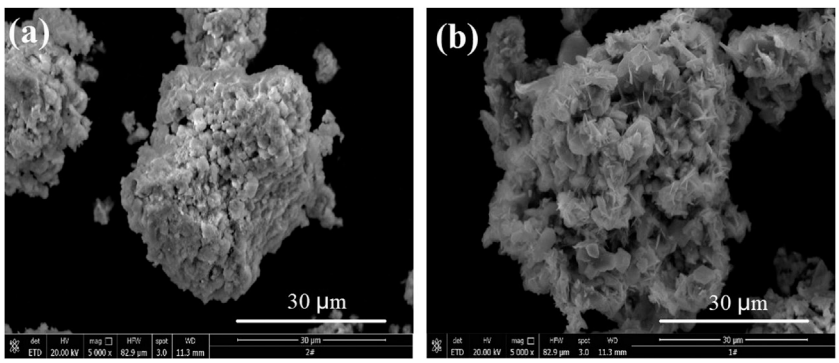

FIGURE 10 | SEM micrograph of the sample and sulfuric acid transition residue.

Leaching Regular Pattern Under Different H_2SO_4 Concentrations

Figure 13A shows that the plots of -ln(1-α) vs. time at different H_2SO_4 concentration. According to the fitting results of **Figure 13A** to plotting the natural logarithm of the apparent rate constant (ln$k$) vs. the natural logarithm of the H_2SO_4 concentration (ln$[H_2SO_4]$), the results can be as presented in **Figure 13B**.

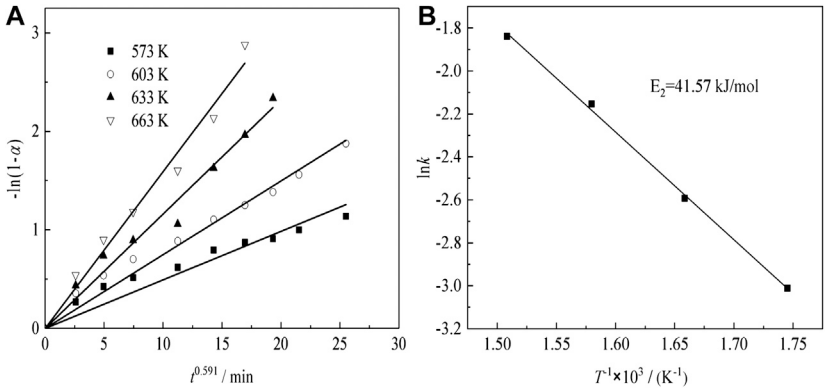

FIGURE 11 | Transformation ratio of Nd and kinetic analysis with various temperatures.

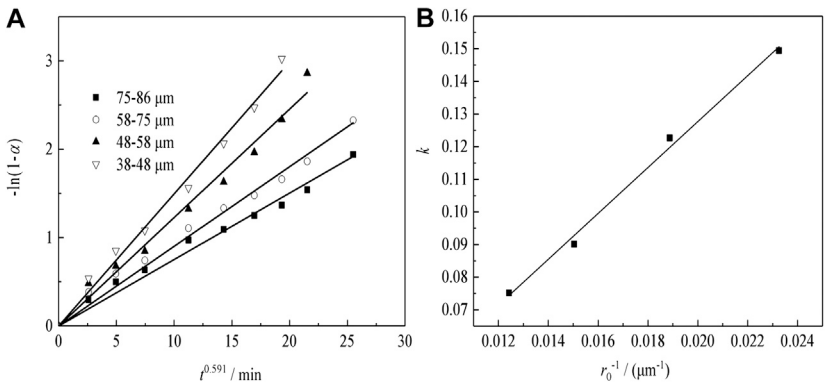

FIGURE 12 | Transformation ratio of Nd and kinetic analysis with various particle sizes.

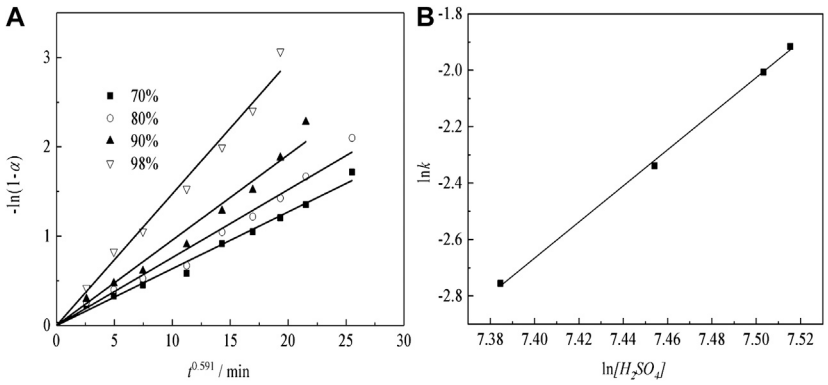

FIGURE 13 | Transformation ratio of Nd and kinetic analysis with various H_2SO_4 concentrations.

The results of sulfuric acid curing for the order of reaction with respect to H_2SO_4 concentration can be obtained. From **Figure 13B**, we obtain that the reaction order for sulfuric acid curing is 6.40. The kinetic equations about the effect of the H_2SO_4 concentration on the Nd transformation ratio can be obtained as **Eq. (5)**:

$$1nk = -50.05 + 6.401n[H_2SO_4] \quad (5)$$

Establishment of Kinetic Mathematical Model

From the above-mentioned analysis, the kinetic equations of sulfuric acid curing can be expressed as **Eq. (6)**:

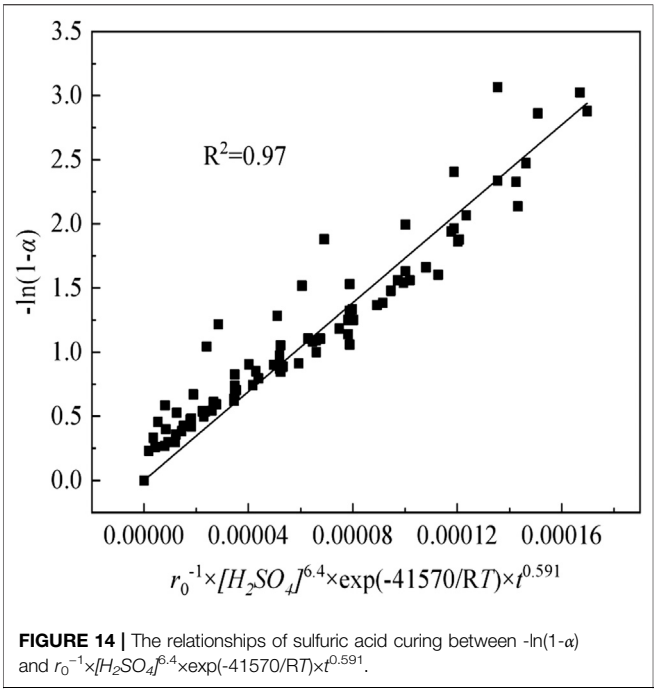

FIGURE 14 | The relationships of sulfuric acid curing between -ln(1-α) and $r_0^{-1}\times[H_2SO_4]^{6.4}\times\exp(-41570/RT)\times t^{0.591}$.

$$-1\mathrm{n}(1-\alpha) = (\mathrm{A}_0/\rho)\times r_0^{-1}\times[H_2SO_4]^{\mathrm{n}}\times\exp(-E/\mathrm{R}T)\times t^{0.591} \quad (6)$$

where, α and other terms have the usual meanings described previously, n represents the reaction order with respect to the H_2SO_4 concentration.

The kinetic parameters are substituted into Eq. (6), and the relationships between -ln(1-α) and $r_0^{-1}\times[H_2SO_4]^{\mathrm{n}}\times\exp(-\mathrm{E}/\mathrm{R}T)\times t^{0.591}$ for sulfuric acid curing are expressed in **Figure 14**. Although the points in the plot show some degree of scatter, straight lines can be fitted to the data with a correlation coefficient (R^2) above 0.97. Therefore, from **Figure 14**, the A_0/ρ of sulfuric acid curing is determined as be 1.73×10^4.

Based on the activation energy, reaction order, and A_0/ρ values previously obtained, the kinetic equations of MHL and EHL can be expressed as **Eq. (7)**:

$$-1\mathrm{n}(1-\alpha) = 1.73\times10^4\times r_0^{-1}\times[H_2SO_4]^{6.4}\times\exp(-41570/\mathrm{R}T)\times t^{0.591} \quad (7)$$

CONCLUSIONS

Herein, the Nd transformation thermodynamics and kinetics of non-magnetic fractions of rare earth molten salt electrolytic slag after magnetic separation by sulfuric acid curing was systematically investigated. According to the analysis of thermodynamic data, the results indicate that with the increase of temperature, the stable range of NdF_3 becomes smaller, while that of Nd^{3+} becomes larger, and the equilibrium constant of the reaction also increases gradually. Compared with the stable range of Nd^{3+} in the potential pH diagram, high temperature is conducive to the transformation of sulfuric acid leaching. Thereafter, the effects of temperature, particle size, and H_2SO_4 concentration on the sulfuric acid curing of sample were investigated. The results indicate that 98% H_2SO_4 can transform neodymium fluoride into neodymium sulfate effectively. Temperature, particle size, and H_2SO_4 concentration have significant effects on the Nd transformation ratio by sulfuric acid curing. Under experimental conditions, the activation energy and the apparent reaction order of the sulfuric acid were determined to be 41.57 kJ mol^{-1} and 6.40, respectively. The results indicate that the sulfuric acid curing process was regulated by the chemical reaction controlling step. Finally, the area of the kinetic equations can be summarized as

$$-1\mathrm{n}(1-\alpha) = 1.73\times10^4\times r_0^{-1}\times[H_2SO_4]^{6.4}\times\exp(-41570/\mathrm{R}T)\times t^{0.591}$$

DATA AVAILABILITY STATEMENT

The original contributions presented in the study are included in the article/Supplementary Material, further inquiries can be directed to the corresponding authors.

AUTHOR CONTRIBUTIONS

LT, JX, XY and LC designed the study, performed the research, analysed data, and wrote the paper. RW and ZX provided ideas and financial support of the study.

FUNDING

Financial support was provided by the National Nature Science Foundation of China (no. 51804136, 52064021, 52074136), China Postdoctoral Science Foundation (No. 2019T120625, 2019M652276), Jiangxi Provincial Cultivation Program for Academic and Technical Leaders of Major Subjects (No. 20204BCJL23031), Jiangxi Province Science Fund for Distinguished Young Scholars (No. 20202ACB213002), Program for Excellent Young Talents, JXUST, Young Jinggang scholars of Jiangxi Province, Merit-based postdoctoral research in Jiangxi Province (No. 2019KY09), and the cultivation project of the State Key Laboratory of Green Development and High-value Utilization of Ionic Rare Earth Resources in Jiangxi Province (No. 20194AFD44003).

ACKNOWLEDGMENTS

First of all, We thank the Institute of Green Metallurgy and Process Intensification, Jiangxi University of Science and Technology, Ganzhou, China, for support of this work. Secondly, we thank all authors for their contribution to this Research Topic. Finally, we would also like to acknowledge the work of the reviewers whose constructive comments contributed to improving the quality of the articles.

REFERENCES

Baláz, P. (2003). Mechanical activation in hydrometallurgy. *Int. J. Miner. Process.* 72 (1–4), 341–354. doi:10.1016/S0301-7516(03)00109-1

Biedermann, R. P. (2014). China's rare earth sector – between domestic consolidation and global hegemony. *Int. J. Emerging Markets* 9 (2), 276–293. doi:10.1108/IJoEM-05-2013-0080

Chen, D. Y., Ouyang, H., Liu, L. C., and Xie, G. (2005). Study on recovery of scrapped molten salt in RE electrolysis. *Jiangxi Metall.* 25 (1), 4–8. doi:10.3969/j.issn.1006-2777.2005.01.002

Chen, Z. H. (2011). Global rare earth resources and scenarios of future rare earth industry. *J. Rare Earth.* 29 (1), 1–6. doi:10.1016/S1002-0721(10)60401-2

Federica, F., Lourdes, Y., Jose, L. A., Bieke, O., and Koen, B. (2019). Integrated process for the recovery of yttrium and europium from CRT phosphor waste. *RSC Adv.* 9 (3), 1378–1386. doi:10.1039/c8ra08158a

Ferron, C. J., and Henry, P. (2016). A review of the recycling of rare earth metals. *Can. Metall. Quart.* 54 (4), 388–394. doi:10.1179/1879139515Y.0000000023

Gao, Z. G., Jia, Z. R., Wang, K. K., Liu, X. H., Bi, L., and Wu, G. L. (2020). Simultaneous enhancement of recoverable energy density and efficiency of lead-free relaxor-ferroelectric BNT-based ceramics. *Chem. Eng. J.* 402, 125951. doi:10.1016/j.cej.2020.125951

He, L. P. (2016). The preparation of neodymium carbonate was recovered from the electrolytic slag of neodymium oxide. *Architectural Eng. Technology Besign* 26, 581. doi:10.3969/j.issn.2095-6630.2016.26.565

Huang, X. W., Li, H. W., Wang, C. F., Wang, G. Z., Xue, X. X., and Zhang, G. C. (2007). Development status and research progress in rare earth industry in China. *Chin. J. Rare Met.* 31 (3), 279–288. doi:10.3969/j.issn.0258-7076.2007.03.002

Huang, X. W., Long, Z. Q., Wang, L. S., and Feng, Z. Y. (2015). Technology development for rare earth cleaner hydrometallurgy in China. *Rare Met.* 34 (4), 215–222. doi:10.1007/s12598-015-0473-x

Kong, M. Y., Jia, Z. R., Wang, B. B., Dou, J. L., Liu, X. H., Dong, Y. H., et al. (2020). Construction of metal-organic framework derived Co/ZnO/$Ti_3C_2T_x$ composites for excellent microwave absorption. *Sustain. Mater. Techno.* 26, e00219. doi:10.1016/j.susmat.2020.e00219

Li, H. G. (1990). *Rare earth metallurgy*. Beijing: Metallurgical Industry Press.

Liang, Y., Li, Y. K., Xue, L. Y., and Zou, Y. (2018). Extraction of rare earth elements from rare earth molten salt electrolytic slag by mineral phase reconstruction. *J. Clean. Prod.* 177, 567–572. doi:10.1016/j.jclepro.2017.12.244

Lin, J., He, Q. P., and Li, C. X. (2012). *A method for separation and recovery of rare earth elements from rare-earth molten salt electrolysis waste*. China Patent CN101956078B.

Onal, M. A. R., and Binnemans, K. (2019). Recovery of RE from waste cathode ray tube (CRT) phosphor powder by selective sulfation roasting and water leaching. *Hydrometallurgy* 183, 60–70. doi:10.1016/j.hydromet.2018.11.005

Shen, L., Wu, N., Zhong, S., and Gao, L. (2017). Overview on China's rare earth industry restructuring and regulation reforms. *J. Resour. Ecol.* 8 (3), 213–222. doi:10.5814/j.issn.1674-764x.2017.03.001

Sokic, M. D., Markovic, B., and Zivkovic, D. (2009). Kinetics of chalcopyrite leaching by sodium nitrate in sulphuric acid. *Hydrometallurgy* 95 (3–4), 273–279. doi:10.1016/j.hydromet.2008.06.012

Tian, L., Xu, Z. F., Chen, L. J., Liu, Y., and Zhang, T. A. (2018). Study on oxygen gas holdup and kinetics using various types of paddles during marmatite leaching process, *Hydrometallurgy* 180, 158–171. doi:10.1016/j.hydromet.2018.06.011

Xiao, Y., Chen, Y. H., and Xu, G. M. (2015). *Separation and recovery method of price components of rare earth praseodymium neodymium electrolysis in molten salt waste*. China Patent CN104805292A.

Yang, Y. M., Wei, T. M., Xiao, M., Niu, F., and Shen, L. T. (2020). Rare earth recovery from fluoride molten-salt electrolytic slag by borax roasting-hydrochloric acid leaching. *JOM* 72 (4), 939–945. doi:10.1007/s11837-019-03732-0

Yurramendi, L., Gijsemans, L., Forte, F., Aldana, J. L., del Río, C., and Binnemans, K. (2019). Enhancing rare-earth recovery from lamp phosphor waste. *Hydrometallurgy* 187, 38–44. doi:10.1016/j.hydromet.2019.04.030

Zhang, H. X., Jia, Z. R., Feng, A. L., Zhou, Z. H., Chen, L., Zhang, C. H., et al. (2020). *In situ* deposition of pitaya-like Fe_3O_4@C magnetic microspheres on reduced graphene oxide nanosheets for electromagnetic wave absorber. *Compos. Part B: Eng.* 199, 108261. doi:10.1016/j.compositesb.2020.108261

Zhang, Y., Wang, Z. Y., Hu, K., Ren, J. H., Yu, N. F., Liu, X., et al. (2021). Anchoring silicon on the basal plane of graphite via a three-phase heterostructure for highly reversible lithium storage. *Energy Storage Mater.* 34, 311–319. doi:10.1016/j.ensm.2020.10.002

Conflict of Interest: The authors declare that the research was conducted in the absence of any commercial or financial relationships that could be construed as a potential conflict of interest.